RSC Advances

ROYAL SOCIETY OF CHEMISTRY

www.rsc.org/advances

Theoretical Study of Fluorination Effect on Charge Transport Properties in Fused Thiophene Derivatives

Jun Yin, Kadali Chaitanya, Xue-Hai Ju*

Key Laboratory of Soft Chemistry and Functional Materials of MOE, School of Chemical Engineering, Nanjing University of Science and Technology, Nanjing 210094, P. R. China

Abstract: To gain a better understanding of the fluorination effect on the charge transport property, the charge transport properties of the six fused thiophene derivatives 2,6-diphenylbisthieno[3,2-b:2',3'-d]thiophene (DP-DTT) 6,6'-diphenyl-2,2'-bibisthieno[3,2-b:2',3'-d]thiophene (DP-BDTT), 2-(pentafluorophenyl)-6-phenylbisthieno[3,2-b:2',3'-d]thiophene (FPP-DTT), 6,6'-bis(pentafluorophenyl)-2,2'-bibisthieno[3,2-b:2',3'-d]thiophene (FPP-BDTT), 2,6-dipentafluorophenyl-bisthieno[3,2-b:2',3'-d]thiophene (DFP-DTT) and 6,6'-dipentafluorophenyl-2,2'-bibisthieno[3,2-b:2',3'-d]thiophene (DFP-BDTT) were explored by the density functional theory (DFT) coupled with the incoherent charge-hopping model at the molecular and crystal levels. The crystal structures of the titled compounds are either predicted by the dispersion-corrected density functional method (DFD-D) or retrieved from the Cambridge Crystallographic Database. Introducing the electron-withdrawing fluorine atoms to the end phenyl of the DTT and BDTT molecules can decrease the HOMO-LUMO gap, which is beneficial to the conductivity. The FPP-BDTT has the largest electron mobility among the six compounds because it has small electron reorganization energy and large transfer integral. The efficient overlaps of

* Corresponding author. E–mail: xhju@njust.edu.cn; Tel: +86 25 84315947-801; fax: +86 25 84431622

π-orbital and smaller π-π stacking distance are proved to be the main reason for its good hole transport property for DFP-DTT. Additionally, FPP-BDTT and DFP-BDTT have shown remarkably anisotropic behaviors and the maximal charge mobilities are along a special crystal axis direction with strong π-π interactions, which further confirms our finding that the fluorination effect may be an effective way to improve the charge mobilities.

Keywords: DFT, fused thiophene derivatives, fluorination effect, charge transport property, π-π interaction

1. Introduction

A growing interest in organic semiconductors has emerged in the past years due to their potential electronic applications in organic light-emitting diodes (OLEDs), organic photovoltaic cells (OPVs) and organic field-effect transistors (OFETs) [1–3]. The advantages of the organic semiconductors such as low cost, easy fabrication, mechanical flexibility, light weight, and large area production, make them good alternatives to conventional inorganic materials [4, 5]. Over the past years, organic π-conjugated materials such as oligothiophenes, linear arenes and their derivatives have been widely studied due to their large π-conjugation and outstanding chemical and physical properties [6–8]. Among the organic semiconductors materials, some representative p-type organic semiconductors have achieved mobility beyond 10 $cm^2 \cdot V^{-1} \cdot s^{-1}$, which can even be compared with the mobility of amorphous silicon devices [9]. On the contrary, the development of n-type organic semiconductors lagged behind of their p-type analogs due to high injection barrier of electron and the intrinsic instability of organic radical anions in the ambient air environment

[10, 11]. Some experimental and theoretical investigations revealed that functionalizing p-type semiconductors with electron-withdrawing groups was a promising way to convert them into n-type ones, such as cyanation, fluorination and chlorination [12, 13]. Hence, the appropriate functionalization is an essential approach to efficiently design and develop high performance n-type organic semiconductors.

To date, many research groups have focused their interests on fused-thiophene based organic semiconductors due to their excellent properties associated with rigid and coplanar conformation via extended conjugation length [14]. Recently, many fused thiophene derivatives were reported to exhibit excellent electrical and charge transport performance [15]. Sun *et al.* have reported a novel organic semiconductor 2,6-diphenylbisthieno[3,2-b:2',3'-d]thiophene (DP-DTT) with a high mobility of 0.42 $cm^2 \cdot V^{-1} \cdot s^{-1}$ using the dithieno[3,2-*b*:2′,3′-*d*]thiophene (DTT) as a skeleton [16]. At the microscopic level, the electron is gained from the electrode to the molecule DP-DTT, the radical anion of DP-DTT will be expected to be involved in a self-exchange electron transfer reaction where an electron hops from an ionized DP-DTT molecule to an adjacent neutral molecule. Chen *et al.* have achieved a high-performance organic semiconductor 6,6'-diphenyl-2,2'-bibisthieno[3,2-b:2',3'-d]thiophene (DP-BDTT) with a mobility of 0.41 $cm^2 \cdot V^{-1} \cdot s^{-1}$ in a single-crystal OFET of bisdithienothiophene-based fused-thiophene (BDTT) [17]. In all the halogenation, the fluorine is the strongest electron-withdrawing atom with an electronegativity of 4.0 according to Pauling definition, which has been demonstrated to be advanced for electron transport as well [18]. Previous studies showed that the n-type or ambipolar organic semiconductors can be obtained by introducing electronegative fluorine atoms to the oligothiophenes [19–21]. As the evidence of this strategy used for this functionalized linear

thiophenes, Chen *et al.* have synthesized asymmetric phenyl and perfluorophenyl end-functionalized dithienothiophene and bisdithienothiophene based fused-thiophene derivatives 2-(pentafluorophenyl)-6-phenylbisthieno[3,2-b:2',3'-d]thiophene (FPP-DTT) and 6,6'-bis(pentafluorophenyl)-2,2'-bibisthieno[3,2-b:2',3'-d]thiophene (FPP-BDTT), which are examined as charge transporting materials [17]. In this regard, we introduced the strong electron-withdrawing fluorine to the asymmetric molecules FPP-DTT and FPP-BDTT to obtain two novel symmetric perfluorophenyl fused-thiophene derivatives 2,6-dipentafluorophenyl-bisthieno[3,2-b:2',3'-d]thiophene (DFP-DTT) and 6,6'-dipentafluorophenyl-2,2'-bibisthieno[3,2-b:2',3'-d]thiophene (DFP-BDTT). For the four fluorinated fused thiophene derivatives, the electron transfer reactions of the radical anion involved an electron hopping to its adjacent neutral molecule instead of loss of fluoride anion. Taking DFP-DTT as an example, when the bond H-F breaking, it needs to absorb the energy of 6.7 eV, while the DFP-DTT accepts an electron, it needs to absorb the energy of only 1.8 eV. Consequently, the H-F bond of DFP-DTT will not break in the electron transfer reaction. The molecular structures of the studied six compounds were depicted in Figure 1.

Up to now, there is still no concise and unambiguous understanding of fluorine interactions, especially for chemical structure, material morphology and macroscopic properties of fluorine compounds. In this work, motivated by the fact that a tiny modification of organic molecules could induce differently optical and electrochemical performances [22], we explored the influence of fluorine substitution on the geometries, electronic properties, and charge transport parameters of the six compounds based on density functional theory (DFT) coupled with incoherent charge-hopping mechanism mode. The present theoretical study will provide ionization potential,

electron affinity, hole extraction potential and electron extraction potential along with the charge transport properties such as charge transfer integral, reorganization energy and charge carrier mobility of those molecules. We hope these discussions can provide a fertile theoretical ground with the rational molecular design and synthesis of the promising organic semiconductors.

2. Theoretical and computational methodology

2.1 Theoretical methodology

In almost all π-conjugated organic materials, the molecular scale charge transport at room temperature occurs via a thermally activated incoherent hopping mechanism [23]. According to the incoherent hopping mechanism, the charge carriers in the crystal structure will jump between two adjacent molecules across the organic layer. The charge transfer rate can be expressed from the Marcus-Hush equation [24]:

$$k = \frac{4\pi^2}{h}\frac{1}{\sqrt{4\pi\lambda k_B T}}V^2 \exp(-\frac{\lambda}{4k_B T}) \quad (1)$$

V denotes the transfer integral between two adjacent molecules in organic single crystal, λ is the reorganization energy, T is the temperature which is 298 K in our calculations, h and k_B are the Planck and Boltzmann constants, respectively.

Generally, the total reorganization energy λ includes contributions from the internal reorganization energy λ_i (induces by the relaxation of molecular geometry) and the external polarization reorganization energy λ_o (derives from the surrounding medium in bulk materials) [25]. For organic solids, the contribution of outer reorganization energy to the total reorganization energy is usually much smaller than that of inner reorganization energy due to weak polar media, so we only focus on the inner reorganization energy here [26]. So, the reorganization energies for

the hole and electron transfers are evaluated using the following formulas [27]:

$$\lambda_h = [E(M^+) - E(M)] + [E^+(M) - E^+(M^+)] \quad (2)$$

$$\lambda_e = [E(M^-) - E(M)] + [E^-(M) - E^-(M^-)] \quad (3)$$

where $E(M)$, $E^+(M^+)$, and $E^-(M^-)$ are the respective energies of optimized neutral, cationic, and anionic structures. $E(M^+)/E(M^-)$ is the neutral energy of the optimized cationic/anionic structure, and $E^+(M)/E(M^-)$ is the cationic/anionic energy of the optimized neutral structure. Besides, the ionic state properties such as vertical ionization potential (IP_V), adiabatic ionization potential (IPa), vertical electron affinities (EA_V), adiabatic electron affinities (EAa), hole extraction potential (HEP) and electron extraction potential (EEP) were calculated by the following formulas [28]:

$$IP_a = E^+(M^+) - E(M)$$

$$IP_V = E^+(M) - E(M)$$

$$EA_a = E(M) - E^-(M^-) \quad (4)$$

$$EA_V = E(M) - E^-(M)$$

$$HEP = E^+(M^+) - E(M^+)$$

$$EEP = E(M^-) - E^-(M^-)$$

The transfer integral V describes the overlap of the electronic wave functions between the donor and acceptor states, which intensively depends on the relatively molecular arrangement in the solid state. The transfer integral is expressed through the site-energy corrected method as [29]:

$$V = \frac{h_{12} - \frac{1}{2}S_{12}(e_1 + e_2)}{1 - S^2{}_{12}} \quad (5)$$

Here, $e_i = \langle \Phi_i | H | \Phi_i \rangle$ (i=1, 2), $h_{12} = \langle \Phi_1 | H | \Phi_2 \rangle$, and $S_{12} = \langle \Phi_1 | S | \Phi_2 \rangle$, where Φ_1 and Φ_2 are the HOMOs/LUMOs of the two monomers in the dimer, H and S are the dimer Hamiltonian and the overlap matrix, respectively.

After obtaining the reorganization energies λ and the transfer integral *V*, the hopping rates were calculated using Equation 1. Here, the charge transport is modeled as a Brownian motion process, as described by a particle diffusion process [30]. The carrier mobility can be obtained by the Einstein equation [31]:

$$\mu = \frac{e}{k_B T} D \tag{6}$$

where μ is the charge carrier mobility, D the isotropic charge diffusion coefficient, and e the electronic charge. Given the hopping rate between the nearest-neighbor molecules, the diffusion coefficient can be evaluated from the hopping rates as [32]

$$D = \frac{1}{2n} \sum_i r_i^2 k_i P_i \tag{7}$$

where n is the dimensionality (when n is equal to 3, we can evaluate the average mobility of all the hopping pathways), k_i the hopping rate due to charge carrier to the *i*th neighbor, r_i the distance to neighbor i, $P_i = k_i (\sum_i k_i)^{-1}$ is the relative probability for charge hopping to the *i*th pathway.

2.2 Computational details

The unit cells of the crystal structures DP-DTT, FPP-DTT, DP-BDTT and FPP-BDTT are retrieved from the Cambridge Crystallographic Database. The crystal structure data of the four compounds are shown in Table S1 in the Supporting Information. Inclusion the dispersion energy (-D) is used to describe the solid-state packing of molecules [33]. Based on this, we performed periodic optimization for the DP-DTT, FPP-DTT, DP-BDTT and FPP-BDTT crystals by using the dispersion-corrected density functional theory (DFT-D) at the LDA/CA-PZ level based on the experimental crystal structures. The optimized crystal structure parameters of the four compounds

were summarized in Table S2. As seen in Table S1 and Table S2, it is noticed that the optimized crystal structure parameters are well consistent with the experiments, which indicates that the method is suitable for the four crystals. Based on this, we also optimized the DFP-DTT and DFP-BDTT crystals by DFT-D method with LDA/CA-PZ functional [34, 35]. The optimized crystal parameters of the DFP-DTT and DFP-BDTT were also summarized in Table S2. All the calculations are performed using the CASTEP code within the Material Studio package [36].

Recent studies have shown the B3LYP hybrid functional at the DFT level is suitable to the oligothiophenes and their derivatives, and hence the monomer geometries of the neutral and ionic states of all the studied molecules were fully optimized by the B3LYP hybrid functional and 6-311G(d,p) basis set [37, 38]. Based on these molecular geometries, the reorganization energies and the ionic state properties were calculated employing the same functional and basis set. The calculations of the above quantities were performed in the Gaussian 09 program package [39]. However, in the calculations of the transfer integral, we chose the PW91 exchange and PW91 correction functionals with 6-31G(d,p) basis set by the site-energy corrected method [40]. Huang *et al.* showed that PW91 functional gave the best description for the bandwidth of organic solid, and some groups also obtained very good results of charge mobilities using PW91PW91/6-31G(d,p) method in the similar investigations [41, 42].

3. Results and discussion

3.1 Crystal and geometric structures

Crystal structure is one of the important properties that determine the charge carrier transport pathways and mobility in organic molecular crystals. The crystal structures of the studied six

compounds were shown in Figure S1. As seen in Figure S1, the DTT moiety in the symmetric DP-DTT is connected with the two end-capped phenyl groups in a slightly bent (arc-shape like) structure. Two phenyl groups are not coplanar to the DTT moiety with torsion angles of about 6º. Note that the DP-DTT is characterized by the herringbone structure. While for the asymmetric FPP-DTT and symmetric DFP-DTT, the fused DTT moiety is nearly coplanar with two end-capped phenyl groups and the unit cells of the two compounds exhibit a face-to face packing motif. For DP-BDTT, two DTT units are paired with each other in the opposite direction to form the BDTT moiety with a slightly twisted structure. Coupled with two phenyl groups with average torsion angles of about 8º, the DP-BDTT exhibited unusual wave shape geometry. It is seen that the symmetric DP-BDTT also exhibits a commonly observed edge-to-face herringbone packing motif as well as DP-DTT, similar to other fused thiophenes in literatures [43, 44]. The fused thiophene DP-BDTT has a herringbone stacking angle of about 43º. On the contrary, for FPP-BDTT and DFP-BDTT, the two DTT units in the BDTT moiety combine in the opposite direction, resulting in a nearly coplanar BDTT moiety. For both FPP-BDTT and DFP-BDTT, the planar molecular structure of the two asymmetric/symmetric materials suggest ideal conditions for the extended π-π interaction of the corresponding molecules, leading to an excellent device performance. These results suggest that that fluorine substitution of the DP-DTT and DP-BDTT have changed the crystal and molecular structure significantly. The electron-withdrawing fluorine substituents make the bent molecules (DP-DTT and DP-BDTT) change to the coplanar molecules (FFP-DTT, DFP-DTT, FFP-BDTT and DFP-BDTT), which is beneficial to a strong π-orbital overlap between adjacent organic molecules in the solid state.

The geometries of the studied molecules have optimized at B3LYP/6-311G(d,p) level of theory in gas phase [37]. The optimized bond lengths, bond angles and dihedral angles as well as their experiment crystal data are shown in Tables S3–S8. As seen the tables, it can be determined that the optimized bond lengths of DP-DTT, FPP-DTT, DP-BDTT and FPP-BDTT are in good agreement with the corresponding experiment values, which indicates that B3LYP functional coupled with the 6-311G(d,p) basis set is appropriate for the geometric properties of the six compounds. Hence, the bond length change upon the reduction and oxidation processes were also obtained from the B3LYP/6-311G(d,p) method. The optimized DP-DTT and DP-BDTT exhibit good coplanarity in the gaseous state, but they display slightly twisted structure in the solid state. Previous investigations revealed that the molecular geometry may be influenced by the intermolecular interaction of neighboring molecules in the solid state. The slightly geometric change, however, appears as not conclusive as regards the method of choice [16, 17]. As seen in Tables S3–S8, the bond length modification is found to take place in the entire molecule due to the extended π-system configurations. Besides, the absolute values of bond lengths between neutral and ionic states are ca. of 0.01 Å with the maximum changes of 0.03 Å for the DP-DTT. By analyzing the optimized geometry of the neutral and ionic states of the studied six molecules, it has been observed that the presence of excess positive and negative charges can not profoundly alter the bond lengths in the substituted DTT and BDTT molecules. Among the compounds, the maximum bond length difference between neutral and ionic states is only 0.023 Å. In order to describe the geometric distortion quantitatively upon carrier transfer processes, we computed the magnitude sum of bond length changes ($\Sigma|\Delta(A\text{-}G)|$ and $\Sigma|\Delta(C\text{-}G)|$) for the six compounds in both charge carrier processes. Here $|\Delta(A\text{-}G)|$ represents the absolute value of bond length difference

between the anionic and neutral geometries, |Δ(C-G)| denotes the absolute value of bond length change between the cationic and neutral ones [45]. The calculated Σ|Δ(A-G)| and Σ|Δ(C-G)| values reach 0.533 Å and 0.321 Å for DP-DTT, 0.490 Å and 0.382 Å for FPP-DTT, 0.456 Å and 0.395 Å for DFP-DTT, 0.579 Å and 0.396 Å for DP-BDTT, 0.555 Å and 0.408 Å for FPP-BDTT, 0.523 Å and 0.423 Å for DFP-BDTT, respectively. The different Σ|Δ(A-G)| and Σ|Δ(C-G)|values in charge transfer processes indicate the six compounds have different geometric modification accompanying the charge transfer process from one molecule to another. As seen from Table S3–S8, the discrepancies of bond angles (Δ*A*) between cation and neutral states are in the range of 0.09–0.87º, and the discrepancies of dihedral angles (Δ*D*) are in the range of 0.05–2.28º, indicating that the geometric deformation in the oxidation process is minor as compared to the reduction process. The variations of dihedral angles from neutral to anion states decrease in the order of DP-DTT > FPP-DTT > DFP-DTT for DTT fused-thiophene derivatives and DP-BDTT > FPP-BDTT > DFP-BDTT for BDTT fused-thiophene derivatives, respectively, indicating a distinct torsion of the anionic structure compared to the planar neutral structure as the number of fluorine atoms increases.

3.2 Reorganization energy

The reorganization energy (λ) is one key parameter governing the hopping rate. It has long been recognized that hole (electron) reorganization energies are closely related to the geometries of cation (anion) states. The molecules with small reorganization energy possess high carrier mobility [46]. The reorganization energies are in proportion to the deformation of the geometries in charge transfer process [42]. The changes of bond lengths between the neutral and ionized

geometries for fused thiophene DTT and BDTT derivatives were presented in Figure S2 and Figure S3. As seen in Figure S2 and Figure S3, the largest deformations of bond lengths for both cation and anion appear on the C-C bond in the thiophene ring. It can also be found that their geometrical deformations accompanying electron transfer are larger, so the electron reorganization energies (λ_e) for the DTT and BDTT derivatives should be larger than the corresponding hole ones (λ_h), which agrees well with the trend of the computed reorganization energy results (see Table 1). The reorganization energies of hole and electron transports of the DTT and BDTT derivatives were obtained through the adiabatic potential (AP) energy surface approach at the B3LYP/6-311G(d,p) level [38]. The reorganization energies of the six compounds were listed in Table 1. From the reorganization energy analysis, DFP-BDTT is expected to have the best hole transport properties, but DP-DTT should possess the smallest electron transfer rate. Among the studied molecule, the DFP-BDTT has the minimum electron reorganization energy of 0.296 eV. The other fluorinated fused-thiophene DTT and BDTT derivatives having less reorganization energy for electron transfer are FPP-BDTT with 0.353 eV, DFP-DTT with 0.399 eV and FPP-DTT with 0.409 eV, respectively. For the DTT derivatives, the λ_h is predicted to decrease in the order of DFP-DTT> FPP-DTT > DP-DTT, while λ_e follows the order of DP-DTT > FPP-DTT > DFP-DTT. The different variation trends of λ_h and λ_e of the DTT derivatives could be explained in terms of geometry changing. The more the geometrical deformation in the charge transfer process is, the larger the λ value is. For the BDTT derivatives, both the λ_h and λ_e are predicted to decrease in the order of DP-DTT > FPP-DTT > DFP-DTT. Additionally, it can be seen that as the number of substituted fluorine atoms increases, the λ_h decreases slightly, and in the meantime the λ_e decreases significantly. From the viewpoint of the reorganization energy, the

introduction of the strong electron-withdrawing fluorine atoms to the end phenyl of DTT and BDTT molecules can significantly influence the geometries of the six compounds and contribute differently to λ_h and λ_e.

3.3 Frontier molecular orbitals

It will be useful to examine the frontier molecular orbitals (FMO) of the six molecules since the FMO is an important factor to affect the carrier transport properties [47]. The relative orderings of the highest occupied orbitals (HOMOs) and the lowest unoccupied orbitals (LUMOs) energies provide a reasonable qualitative indication of the ability of hole and electron injection and also determine the redox stability of organic semiconductors [29]. The smaller the injection barrier is, the more easily the charges are injected. The energies of HOMOs and LUMOs as well as the energy gaps of all the studied molecules were shown in Figure 2 and their corresponding distribution of the FMOs were presented in Figure 3. As can be seen from Figure 3, the electron distribution of the HOMOs or LUMOs for the six systems is similar. For the symmetric molecules DP-DTT, DP-DFP, DP-BDTT and DP-BDTT, the LUMOs denote symmetrical distributions, while the HOMOs present asymmetrical distributions. It was found that all the LUMOs possess π orbital features and spread over the thiophene moieties and the HOMOs are mainly localized on the carbon atoms. As observed in the four molecules, the sulfur atom has only an imperceptible contribution to the HOMOs, but it contributes more to the LUMOs. The more uniform distribution of LUMOs for the symmetrical molecules suggests that electron delocalizations of these molecules are better compared to the unsymmetrical molecules FPP-DTT and FPP-BDTT. As seen in Figure 2, the molecular orbitals of the substituted DTT and BDTT derivatives are more

stabilized since they have relatively lower LUMO energy levels compared with the unsubstituted molecule DP-DTT and DP-BDTT. The low LUMO levels facilitate electron injection that is necessary for a stable n-type organic semiconductor in the environment. With reference to the conductivity, the energy gap of HOMO-LUMO (E_{gap}) can be considered approximately as the band gap energy [48]. The smaller E_{gap} is, the larger the conductivity is. Obviously, the E_{gap} of DFP-BDTT (2.28 eV) is smaller than those of other compounds. This is beneficial to the conductivity efficiently. It is noted that with increasing numbers of the substituted fluorine atoms, the LUMO energy of the DTT/BDTT derivative decreases and the HOMO energy also decreases but not as much as the LUMO, indicating that the fluorination should be beneficial to electron injection. In order to probe the reduction of FMO energies, we analyzed the natural bond orbital (NBO) charges of compounds DP-DTT and its fluorinated derivative DFP-DTT (seen in Figure 4). As shown in Figure 4, the charges at perfluorphenyl carbon atoms of DFP-DTT are 0.075 to 0.168 electrons, while those of DP-DTT are –0.174 to –0.312 electrons. Additionally, the electron occupancy on C-C bond (1.966 to 3.635) in the perfluorphenyl of DFP-DTT is smaller than those in phenyl of DP-DTT (1.969 to 3.646). This means that the electrons are transferred from carbon to fluorine atoms during fluorination. The contributions of atomic orbitals to the HOMO and LUMO for DP-DTT and DFP-DTT are presented in Figure S4. The contributions of the fluorine atoms to the LUMO and HOMO for DFP-DTT are 0.07%–0.59% and 0.04%–0.53%, respectively. While the contributions of the corresponding hydrogen atoms to LUMO and HOMO for DP-DTT are 0.001%–0.04% and 0.004%–0.04%, respectively. Moreover, the electronegativity of fluorine is greater. Thus, the strong attraction of fluorine nuclei to electron lowers the potential energy of electron. The second-order perturbation estimates of “donor–acceptor” interactions in the NBO

basis. This is carried out by examining all possible interactions between "filled" (donor) Lewis-type NBOs and "empty" (acceptor) non-Lewis NBOs, and estimating their stabilization energy by second order perturbation theory [49]. The stabilization energies E(2) are proportional to the NBO interacting intensities [50]. The NBO analysis shows that the orbital interaction F→C between the fluorine and its corresponding ortho carbon atom in the phenyl of the DFP-DTT has a stabilization energy as large as 4.78 kcal/mol, while the interactions of the DP-DTT and CH3CH3CHF are less than a default threshold of 0.5 kcal/mol. The Wiberg's bond index calculated at the B3LYP/6-311G (d) level for the C-F bond between fluorine atom and phenyl ring of DFP-DTT is 0.9176, while that of CH3CH3CHF is 0.6371, which further indicates that there are p-π conjugations between F and phenyl. On the whole, the decrease of HOMO and LUMO energies by the fluorination is not only attributed to the π-conjugation extension to fluorinated phenyl groups, but also to the electron-withdrawing effect of the fluorine atoms.

3.4 Electron affinities (EA) and ionization potentials (IP)

To inject an electron into the LUMO efficiently, EA must be high enough, which is an important requirement of an excellent n-type organic semiconductor. On the contrary, IP must be low enough to allow an efficient hole injection into the HOMO [51]. The IP, EA, both vertical and adiabatic, and extraction potentials (HEP and EEP for the hole and electron, respectively) were calculated by the Equation 4 and the results were summarized in Table 1. The small difference in the vertical and adiabatic values indicates that the structural relaxation upon charge injection is small. It has been observed that the ionization potentials for vertical excitations of the DTT fused-thiophene derivatives follow the order of DFP-DTT > FPP-DTT > DP-DTT and the IP_V of

values of the BDTT derivatives are predicted to decrease in the order of DFP-BDTT > FPP-BDTT > DP-BDTT. The orders of EA_a of DTT derivatives are DFP-DTT (1.553 eV) > FPP-DTT (1.226 eV) > DP-DTT (0.867 eV) and the EA_a of BDTT derivatives follows DFP-BDTT (1.860 eV) > FPP-BDTT (1.627 eV) > DP-BDTT (1.376eV). Obviously, the introduction of fluorine substituents to the DTT/BDTT increases the ionization potential and electron affinity. The EA_a values of DP-BDTT, FPP-DTT and DP-DTT are small, suggesting that three compounds have a large barrier for electron injection. The large EA_a values of DFP-BDTT give rise to high stability of its radical anions in ambient atmosphere, which is an important requirement of fine n-type OFET material [52]. Some investigations showed that the EAa value should be greater than 2.8 eV for air-stable n-channel materials due to the inherent instability of organic anions in air [53]. Hence, the DFP-BDTT is ill-suited to being used as electron transport materials for their low air-stability. As observed for HEP, DP-BDTT has minimum HEP of 5.948 eV, which demonstrates that the injection of hole into DP-BDTT is easier than in other molecules. On the contrary, DFP-BDTT has maximum EEP of 2.004 eV, indicating that the injection of electron into the DFP-BDTT becomes easier. The above results show that the substitution of electron-withdrawing fluorine atoms can significantly affect the electron-transporting properties of DTT and BDTT fused-thiophene derivatives.

3.5 Transfer integral and packing motif

It is well known that the charge transport properties of conjugated molecules critically depend on the transfer integrals, which are highly sensitive to the relative orientations of the adjacent molecules and their crystal packing motifs [54]. To better understand the transfer

integrals, it is necessary to investigate the crystal structures of the studied compounds. As seen from the Figure S1, DP-DTT, FFP-DTT and DFP-DTT crystallize in a monoclinic space group P21/c, while DP-BDTT, FFP-BDTT and DFP-BDTT crystallize in a triclinic space group P-1 [55–57]. For the DP-DTT and DP-BDTT, the molecular stack forms a herringbone structure in the *a*-*b* plane, there is no π-π overlap along the *b* axis. For the other four fluorinated crystalline structures, the molecular stacking forms a face-to-face structure in the *a*-*c* plane with the π-π stacking between consecutive molecules along the *c* axis, indicating that the attachment of fluorine atoms to the DTT/BDTT skeleton can effectively convert the herringbone packing to the π-π stacking. Based on the crystal structures, the main carrier hopping pathways of all the investigated compounds were depicted in the Figure 5. The packing motifs of dimer P1 for DP-DTT and DP-BDTT manifest a slipped face-to-face π-π stacking, which is considered to be a favorable packing motif with small energetic disorder and beneficial topology of charge percolating network [58, 59]. The arrangement of dimers P3 and P5 of the two crystals are completely shifted with little intermolecular overlap or the edge-to-edge packing. The transfer integral V was evaluated from the dimer in the packing pathway and the results for both hole (V_h) and electron (V_e) were given in Table 2. It is generally accepted that the transfer integral between two molecules is closely related to the intermolecular interactions [60]. The transfer integrals of all hopping pathways were calculated by the site-energy corrected method at PW91PW91/6-31G(d,p) level, which has been proven to give reliable estimation of transfer integral for conjugated organic compounds [42]. It can be seen from Table 2, there is a certain relation between the molecular centroid to centroid distance (d) in dimer and transfer integral (V). The transfer integral depends on the distance of the intermolecular moieties directly interacting with each other. Usually, the

transfer integral always become larger with a shorter *d* in the dimer. When the *d* value is too large, the transfer integral approaches zoo. Besides, for the studied compounds except DP-DTT and DP-BDTT, the transfer integral of hole is larger than that of electron, indicating that four compounds are beneficial to hole transfer from the viewpoint of transfer integral. Interestingly, the V_e and V_h of the π-π stacking P1 are not the largest one in DP-DTT and DP-BDTT, whereas the edge-to-edge pathways P3 and P5 lead to the largest V_e and V_h, which can be explained by the fact although dimers P1 and P2 adopt a π-π stacking, they have large *d* distances, which results in a small overlap between the orbitals of the neighboring molecules. As seen from Table 2, with the introduction the fluorine atoms to the end phenyl of DTT and BDTT derivatives, the largest V_e and V_h of the fluorinated fused-thiophene compounds increase significantly, especially the value of the V_h. To further understand the intermolecular effective electronic couplings, the overlap of LUMO orbitals of the dimer with the maximal transfer integral for the DP-DTT and DFP-DTT are presented in Figure 6. As seen Figure 6, in comparison with the unfluorinated dimer of DP-DTT, dimer P7 for the DFP-DTT adopts the perfect π-π stacking. It is noted that both dimers P5 and P7 are composed of the relevant molecular orbitals of the isolated monomer, and the dimer of the fluorinated DFP-DTT have relatively larger electron transfer value between the neighboring molecules than the unfluorinated molecule DP-DTT, indicating further that the transport path along the perfect π-π stacking direction is the best transfer pathway for electron transport. The above results also shed light on the larger overlap area of the π-π stacking and the smaller vertical distance between neighboring molecules contribute to the larger transfer integrals.

3.6 Charge carrier mobility and anisotropic mobility

As can be seen from Table 1 and Table 2, the calculated reorganization energies of hole and electron transfers for the six compounds are larger than the largest hole and electron transfer integrals, we could therefore be convinced that the localized description of the charge transfer by the Marcus–Hush model is adequate for investigating the charge mobilities of the six compounds [42, 61]. Based on the calculated reorganization energy and transfer integral, the carrier mobility for both hole and electron are evaluated at 298K using the Equations 1, 5 and 6 and the results are given in Table 3. It can be found that these molecular crystals almost possess larger hole mobilities within the range from 0.01 to 0.709 $cm^2 \cdot V^{-1} \cdot s^{-1}$ in comparison with the corresponding electron mobilities, indicating that the DTT and BDTT fused-thiophene derivatives should be a class of candidates for the *p*-type organic semiconductors. Obviously, the predicted the values of hole mobility (μ_h) for the fluorine substituted molecules are more than 0.1 $cm^2 \cdot V^{-1} \cdot s^{-1}$, the threshold value fully meeting the practical OFET application. However, the μ_h of the DP-DTT is 0.01 $cm^2 \cdot V^{-1} \cdot s^{-1}$ from the hoping model, less than the experimental value of 0.41 $cm^2 \cdot V^{-1} \cdot s^{-1}$. The discrepancy between the theoretical and experiment value is accepted since the charge carrier mobility is influence by many factors during facbrication and measurement, and the resultant consequences often change in some range [62, 63]. Among the DTT derivatives, both μ_h and μ_e vary as DFP-DTT > FPP-DTT > DP-DTT. For the series BDTT derivatives, the μ_h decreases in the order of DFP-BDTT > FPP-BDTT > DP-BDTT, and μ_e follows the order of FPP-BDTT > DFP-BDTT > DP-BDTT. Obviously, the electron-withdrawing fluorine substituted π-conjugated molecules have the relatively large mobilities due to the large and direct π-π overlap and the lower molecular orbital energy levels, which is favorable for obtaining high-performance n-type organic semiconductor materials. As for the DP-DTT and DP-BDTT, the herringbone structures lead to

smaller hole and electron mobility. On the other hand, the calculated μ_e of DP-BDTT is 0.019 $cm^2 \cdot V^{-1} \cdot s^{-1}$, slightly larger than μ_h of 0.015 $cm^2 \cdot V^{-1} \cdot s^{-1}$, indicating that the DP-BDTT may be an electron-dominated ambipolar transport material. Judged by the charge carrier mobilities of these compounds, it can be seen that the attachment of fluorine atoms to the end phenyl of fused-thiophene DTT/BDTT derivatives can change the packing motif and increase the π-π overlap to achieve high charge mobility and enhance the performance of the organic semiconductors.

The directional dependence of the mobility, namely the anisotropy of mobility, is also an important factor that leads to the disagreement between the experimental and theoretical data [42]. As can be seen in Table 3, we speculated that the charge transports in DP-DTT, DP-BDTT, FPP-BDTT and DFP-BDTT crystals are remarkably anisotropic. Understanding the anisotropy of the mobility can help control the orientation of transistor channel relative to the reference axis of molecular crystal. The angular resolution anisotropic mobility can be calculated by the following equation [64]:

$$\mu_{\Phi} = \frac{e}{2k_B T} \sum_i d_i^{\,2} k_i P_i \cos^2 \gamma_i \cos^2(\theta_i - \Phi)$$

where Φ is the orientation angle of the transistor channel relative to the reference crystallographic axis, and θ_i and γ_i are the angle of the projected hopping paths of different dimers relative to the reference axis. We only considered dimer P in the mobility orientation function on the basal stacked layer due to the smaller transfer integrals along transfer pathways in dimers T1 and T2 in these four compounds, that is, γ_i =0°. Thus, the angular resolution anisotropic hole and electron mobilities of DP-DTT and DFP-BDTT are depicted in Figure 7 and Figure 8 and the anisotropic mobilities of DP-BDTT and FPP-BDTT are presented in Figure S5 and S6. The anisotropy of hole

mobility in DP-DTT exhibit anisotropic behavior, while the electron mobility is closely isotropic. On the contrary, the DP-BDTT crystal exhibits remarkable angular dependence and anisotropic behavior in electron mobility, while the hole electron mobility for DP-BDTT is closely isotropic. In addition, DP-BDTT has the highest electron mobility (0.023 $cm^2 \cdot V^{-1} \cdot s^{-1}$) at the reference angle of 45º and 225º. The projections of their hopping pathways possessing the maximal transfer integrals are along the above directions. As for FPP-BDTT and DFP-BDTT, the two molecular crystals exhibit remarkable angular dependence and anisotropic behaviors in electron and hole mobilities. For FPP-BDTT, at the reference angles of 90º and 270º, the largest hole and electron mobilities are 0.95 and 0.12 $cm^2 \cdot V^{-1} \cdot s^{-1}$, corresponding to the transport pathways with π-π intermolecular interactions along the *b* axis. However, the minima appear along the *a* axis, which corresponds to the reference angle of 0º and 180º. The largest hole and mobilities for DFP-BDTT are 1.05 and 0.11 $cm^2 \cdot V^{-1} \cdot s^{-1}$, corresponding to the parallel direction of *b* crystallographic axis (along the T2 direction). The directions of the lowest hole and electron mobilities of DFP-BDTT are also perpendicular to the axis in the *a*-*b* plane. According to Figure S5 and Figure S6, it is also found that that the directions of highest hole and electron mobilities correspond to the transport pathways possessing large transfer integrals. It should be noticed that the large anisotropic charge carrier mobilities found in the four crystals in this work may be quite useful for the fabrication of high-performance OFET devices.

4. Conclusions

In this work, we have presented a computational investigation of the DTT and BDTT fused-thiophene derivatives based upon the DFT calculations coupled with the charge-hopping

mechanism aimed to elucidate the charge transport properties of these six compounds. The molecular geometry, reorganization energy, frontier orbitals, IPs and EAs, transfer integrals, charge mobility as well as anisotropic mobility have been explored. As the hydrogen atoms of end phenyl were substituted by fluorine atoms, the LUMO energy levels lower obviously, which indicates that the introduction of the fluorine atoms to the studied molecules should be beneficial to electron injection. The analysis of the reorganization energy demonstrates that both hole and electron reorganization energies decrease as the number of the substituent fluorine atoms increase, indicating that the fluorination may be an efficient method to obtain high mobility. The discussion of transfer integrals suggests that the charge transport properties are mainly determined by pathways containing intermolecular π-π interactions. The larger overlap area of the π-π stacking and the smaller vertical distance between neighboring molecules will contribute to the larger transfer integrals. The fluorinated DTT and BDTT compounds with the small reorganization energy and larger transfer integral have the relatively charge mobility compared with the unsubstituted DP-DTT and DP-BDTT. The simulation for the angle dependence of mobility reveals that perfluorophenyl fused-thiophene derivatives FPP-BDTT and DFP-BDTT have remarkably anisotropic behaviors and the maximal charge mobilities are along a special crystal axis with strong π-π interactions. Fluorination of DP-DTT and DP-BDTT could be an effective way to improve their carrier mobilities.

Acknowledgements

The authors thank the National Science Foundation of China (No. 21372116) as well as the Project Funded by the Priority Academic Program Development of Jiangsu Higher Education

Institutions (PAPD) for supporting this work.

References

[1] H. L. Dong, C. L. Wang and W. P. Hu, *Chem. Commun.*, 2010, **46**, 5211.

[2] A. C. Grimsdale, K. L. Chan, R. E. Martin, P. G. Jokisz and A. B. Holmes, *Chem. Rev.*, 2009, **109**, 897.

[3] A. W. Hains, Z. Q. Liang, M. A. Woodhouse and B. A. Gregg, *Chem. Rev.,* 2010, **110**, 6689.

[4] A. Facchetti, *Mater. Today.*, 2007, **10**, 28.

[5] M. Mas-Torrent and C. Rovira, *Chem. Soc. Rev.*, 2008, **37**, 827.

[6] H. Meng, F. Sun, M. B. Goldfinger, G. D. Jaycox, Z. Li, W. J. Marshall and G. S. Blackman, *J. Am. Chem. Soc.*, 2005, **127**, 2406.

[7] R. Rybakiewicz, I. Tszydel, J. Zapala, L. Skorka, D. Wamil, D. Djurado, J. Pécaut, J. Ulanski, M. Zagorska and A. Pron, *RSC. Adv*., 2014, **4**, 14089.

[8] X. D. Tang, Y. Liao, H. Geng and Z. G. Shuai, *J. Mater. Chem.*, 2012, **22**, 18181.

[9] V. Podzorov, E. Menard, A. Borissov, V. Kiryukhin, J. A. Rogers and M. E. Gershenson, *Phys. Rev. Lett.*, 2004, **93**, 86602.

[10] C. Huang, J. E. West and H. E. Katz, *Adv. Funct. Mater.*, 2007, **17**, 142.

[11] H. Ebata, T. Izawa, E. Miyazaki, K. Takimiya, M. Ikeda, H. Kuwabara and T. Yui, *J. Am. Chem. Soc.*, 2007, **129**, 15732.

[12] S. Subramanian, S. K. Park, S. R. Parkin, V. Podzorov, T. N. Jackson and J. E. Anthony, *J. Am. Chem. Soc.*, 2008, **130**, 2706.

[13] S. Chai, S. H. Wen, J. D. Huang and K. L. Han, *J. Comput. Chem.*, 2011, 3218.

[14] H. H. Fong, V. A. Pozdin, A. Amassian, G. G. Malliaras, D. M. Smilgies, M. Q. He, S. Gasper,

F. Zhang and M. Sorensen, *J. Am. Chem. Soc.*, 2008, **130**, 13202.

[15] W. P. Wu, Y. Q. Liu and D. B. Zhu, *Chem. Soc. Rev.*, 2010, **39**, 1489.

[16] Y. Sun, Y. Ma, Y. Liu, Y. Lin, Z. Wang, Y. Wang, C. Di, K. Xiao, X. Chen, W. Qiu, B. Zhang, G. Yu, W. Hu and D. B. Zhu, *Adv. Funct. Mater.*, 2006, **16**, 426.

[17] M. C. Chen, S. Vegiraju, C. M. Huang, P. Y. Huang, K. Prabakaran, S. L. Yau, W. C. Chen, W. T. Peng, I. Chao, C. Kim and Y. T. Tao, *J. Mater. Chem. C*, 2014, **2**, 8892.

[18] Y. F. Lim, Y. Shu, S. R. Parkin, J. E. Anthony and G. G. Malliaras, *J. Mater. Chem.*, 2009, **19**, 3049.

[19] B. Stadlober, M. Zirkl, M. Beutl and G. Leising, *Appl. Phys. Lett.*, 2005, **86**, 242902.

[20] R. Schmidt, M. M. Ling, J. H. Oh, M. Winkler, M. Könemann, Z. N. Bao and F. Würthner, *Adv. Mater.*, 2007, **19**, 3692.

[21] J. Kim, H. M. Ko, N. Cho, S. Paek, J. K. Lee and J. Ko, *RSC. Adv*., 2012, **2**, 2692.

[22] Y. A. Duan, H. B. Li, Y. Geng, Y. Wu, G. Y. Wang and Z. M. Su, *Org. Electron.*, 2014, **15**, 602.

[23] J. L. Brédas, D. Beljonne, V. Coropceanu and J. Cornil, *Chem. Rev.*, 2004, **104**, 4971.

[24] R. A. Marcus, *Rev. Mod. Phys.*, 1993, **65**, 599.

[25] S. Di Motta, E. Di Donato, F. Negri, G. Orlandi, D. Fazzi and C. Castiglioni, *J. Am. Chem. Soc.*, 2009, **131**, 6591.

[26] D. P. McMahon, *J. Phys. Chem. Lett.*, 2010, **1**, 941.

[27] H. L. Tavernier and M. D. Fayer, *J. Phys. Chem. B*, 2000, **104**, 11541.

[28] G. Saranya, K. Navamani and K. Senthilkumar, *Chem. Phys.*, 2014, **433**, 48.

[29] V. Coropceanu, J. Cornil, D. A. da Silva Filho, Y. Olivier, R. Silbey and J. L. Bredas, *Chem.*

Rev., 2007, **107**, 926.

[30] L. B. Schein and A. R. McGhie, *Phys. Rev. B*, 1979, **20**, 1631.

[31] P. Raghunath, M. A. Reddy, C. Gouri, K. Bhanuprakash and V. J. Rao, *J. Phys. Chem. A*, 2006, **110**, 1152.

[32] W. Q. Deng and W. A. Goddard III, *J. Phys. Chem. B*, 2004, **108**, 8614.

[33] F. Ortmann, F. Bechstedt and W. G. Schmidt, *Phys. Rev. B*, 2006, **73**, 205101.

[34] V. B. Deyirmenjian, V. Heine, M. C. Payne, V. Milman, R. M. Lynden-Bell and M. W. Finnis, *Phys. Rev. B*, 1995, **52**, 15191.

[35] M. Cococcioni and S. de Gironcoli, *Phys. Rev. B*, 2005, **71**, 035105.

[36] J. P. Perdew, J. A. Chevary, S. H. Vosko, K. A. Jackson, M. R. Pederson, D. J. Singh and C. Fiolhais, *Phys. Rev. B*, 1992, **46**, 6671.

[37] A. A. El-Azhary and H. U. Suter, *J. Phys. Chem.*, 1996, **100**, 15056.

[38] P. Song and F. C. Ma, *J. Phys. Chem. A*, 2010, **114**, 2230.

[39] M. J. Frisch, G. W. Trucks, H. B. Schlegel, G. E. Scuseria, M. A. Robb, J. R. Cheeseman, G. Scalmani, V. Barone, B. Mennucci, G. A. Petersson, H. Nakatsuji, M. Caricato, X. Li, H. P. Hratchian, A. F. Izmaylov, J. Bloino, G. Zheng, J. L. Sonnenberg, M. Hada, M. Ehara, K. Toyota, R. Fukuda, J. Hasegawa, M. Ishida, T. Nakajima, Y. Honda, O. Kitao, H. Nakai, T. Vreven, J. A. Montgomery, Jr., J. E. Peralta, F. Ogliaro, M. Bearpark, J. J. Heyd, E. Brothers, K. N. Kudin, V. N. Staroverov, R. Kobayashi, J. Normand, K. Raghavachari, A. Rendell, J. C. Burant, S. S. Iyengar, J. Tomasi, M. Cossi, N. Rega, J. M. Millam, M. Klene, J. E. Knox, J. B. Cross, V. Bakken, C. Adamo, J. Jaramillo, R. Gomperts, R. E. Stratmann, O. Yazyev, A. J. Austin, R. Cammi, C. Pomelli, J. W. Ochterski, R. L. Martin, K. Morokuma, V. G.

Zakrzewski, G. A. Voth, P. Salvador, J. J. Dannenberg, S. Dapprich, A. D. Daniels, O. Farkas, J. B. Foresman, J. V. Ortiz, J. Cioslowski, and D. J. Fox, *Gaussian 09, Revision A.02*, Gaussian, Inc., Wallingford CT, 2009.

[40] X. K. Chen, J. F. Guo, L. Y. Zou, A. M. Ren and J. X. Fan, *J. Phys. Chem. C*, 2011, **115**, 21416.

[41] J.S. Huang and M. Kertesz, *J. Chem. Phys.*, 2005, **122**, 234707.

[42] M. C. R. Delgado, E. G. Kim, D. A. da Silva Filho and J. L. Bredas, *J. Am. Chem. Soc.*, 2010, **132**, 3375.

[43] J. Youn, P. Y. Huang, S. Zhang, C.-W. Liu, S. Vegiraju, K. Prabakaran, C. Stern, C. Kim, M. C. Chen, A. Facchetti and T. J. Marks, *J. Mater. Chem. C*, 2014, **2**, 7599.

[44] J. H. Gao, R. J. Li, L. Q. Li, Q. Meng, H. Jiang, H. X. Li and W. P. Hu, *Adv. Mater.*, 2007, **19**, 3008.

[45] C. B. Zhao, W. L. Wang, S. W. Yin and Y. Ma, *New J. Chem.*, 2013, **37**, 2925.

[46] R. Nithya and K. Senthilkumar, *Org. Electron.*, 2014, **15**, 1607.

[47] S. S. Zade and M. Bendikov, *Chem. Eur. J.*, 2008, **14**, 6734.

[48] X. D. Tang, Y. Liao, H. Z. Gao, Y. Geng and Z. M. Su, *J. Mater. Chem.*, 2012, **22**, 6907.

[49] J. P. Foster and F. Weinhold, *J. Am. Chem. Soc.*, 1980, **102**, 7211.

[50] A. J. Lopes-Jesus, M. T. S. Rosado, I. Reva, R. Fausto, M. E. S. Eusébio and J. S. Redinha, *J. Phys. Chem. A*, 2008, **112**, 4669.

[51] H. G. Liu, J. L. Mu and J. Y. Lee, *J. Phys. Chem. B*, 2011, **115**, 8409.

[52] J. Yin, K. Chaitanya and X. H. Ju, *J. Mater. Chem. C*, 2015, **3**, 3472.

[53] Y. C. Chang, M. Y. Kuo, C. P. Chen, H. F. Lu and I. Chao, *J. Phys. Chem. C*, 2010, **114**,

11595.

[54] C. R. Newman, C. D. Frisbie, , J. L. Brédas, P. C. Ewbank and K. R. Mann, *Chem. Mater.*, 2004, **16**, 4436.

[55] Y. Sun, Y. Ma, Y. Liu, Y. Lin, Z. Wang, Y. Wang, C. Di, K. Xiao, X. Chen, W. Qiu, B. Zhang, G. Yu, W. Hu and D. B. Zhu, *Adv. Funct. Mater.*, 2006, **16**, 426.

[56] C. Kim, M. C. Chen, Y. J. Chiang, Y. J. Guo, J. Youn, H. Huang, Y. J. Liang, Y. J. Lin, Y. W. Huang, T. S. Hu, G. H. Lee, A. Facchetti and T. J. Marks, *Org. Electron.*, 2010, **11**, 801

[57] P. Y. Huang, L. H. Chen, C. Kim, H. C. Chang, Y. J. Liang, C. Y. Feng, C. M. Yeh, J. C. Ho, C. C. Lee and M. C. Chen, *ACS Appl. Mater. Interfaces*, 2012, **4**, 6992.

[58] S. E. Koh, C. Risko, D. A. da Silva Filho, O. Kwon, A. Facchetti, J. L. Bredas, T. J. Marks and M. Ratner, *Adv. Funct. Mater.*, 2008, **18**, 332.

[59] G. J. Nan and Z. S. Li, *Org. Electron.*, 2012, **13**, 1229.

[60] M. Schrader, R. Fitzner, M. Hein, C. Elschner, B. Baumeier, K. Leo, M. Riede, P. Bäuerle and D. Andrienko, *J. Am. Chem. Soc.*, 2012, **134**, 6052.

[61] S. F. Zhang, X. K. Chen, J. X. Fan and A. M. Ren, *Org. Electron.*, 2013, **14**, 607.

[62] G. Nan, L. Wang, X. Yang, Z. G. Shuai and Y. Zhao, *J. Chem. Phys.*, 2009, **130**, 024704

[63] B. Zhang, Y. H. Kan, Y. Geng, Y. A. Duan, H. B. Li, J. Hua and Z. M. Su, *Org. Electron.*, 2013, **14**, 1359.

[64] S. H. Wen, A. Li, J. Song, W. Q. Deng, K. L. Han and W. A. Goddard Ⅲ, *J. Phys. Chem. B*, 2009, **113**, 8813.

Table 1. The calculated ionization potentials, electron affinities (adiabatic and vertical), hole extraction potential and electron extraction potential and reorganization energies for the studied **DTT** and **BDTT** derivatives at the B3LYP/6-311G(d,p) level (All energies are in eV)

Compound	IP_v	IP_a	EA_v	EA_a	HEP	EEP	λ_h	λ_e
DP-DTT	6.713	6.547	0.618	0.867	6.394	1.045	0.319	0.427
DP-BDTT	6.266	6.087	1.165	1.376	5.948	1.540	0.318	0.375
FPP-DTT	7.011	6.837	0.998	1.226	6.682	1.407	0.329	0.409
FPP-BDTT	6.456	6.278	1.430	1.627	6.139	1.782	0.317	0.353
DFP-DTT	7.318	7.142	1.337	1.553	6.986	1.736	0.332	0.399
DFP-BDTT	6.605	6.471	1.707	1.860	6.340	2.004	0.265	0.296

Table 2. The hole (V_h) and electronic (V_e) transfer integrals (meV) and distances (Å) of main carrier hopping pathways selected based on the crystal structures for **DTT** and **BDTT** derivatives

Compound	Pathways	d [a]	V_h [b]	V_e [b]
DP-DTT	P1 and P2	5.92	–1.50	21.40
	P3 and P4	4.73	–20.70	23.40
	P5 and P6	4.73	–20.70	23.40
DP-BDTT	P1 and P2	5.96	–0.90	14.70
	P3 and P4	4.79	–22.40	31.70
	P5 and P6	4.80	–22.70	30.70
FPP-DTT	P1 and P2	5.87	4.10	10.70
	P3 and P4	6.88	0.20	4.40
	P5 and P6	9.39	0.00	–0.30
	P7 and P8	3.76	–174.40	68.11
FPP-BDTT	P1 and P2	5.83	2.90	26.50
	P3 and P4	6.81	0.00	4.90
	P5 and P6	3.83	151.16	61.11
	P7 and P8	7.14	0.10	1.20
DFP-DTT	P1 and P2	6.04	6.70	–11.50
	P3 and P4	7.13	0.30	3.10
	P5 and P6	9.67	0.00	–0.20
	P7 and P8	3.78	–162.88	66.71
DFP-BDTT	P1 and P2	5.97	–2.50	10.90
	P3 and P4	7.03	0.00	5.50
	P5 and P6	3.87	–141.35	54.10

[a] The values of d refer to centroid to centroid distances

[b] The transfer integrals calculated at PW91PW91/6-31G(d,p) level

Table 3. The calculated hole and electron mobilities (μ_h and μ_e, in $cm^2 \cdot V^{-1} \cdot s^{-1}$) for the **DTT** and **BDTT** derivatives

Compound	μ_h	μ_e
DP-DTT	0.010	0.008
DP-BDTT	0.015	0.019
FPP-DTT	0.581	0.057
FPP-BDTT	0.637	0.087
DFP-DTT	0.709	0.058
DFP-BDTT	0.699	0.075

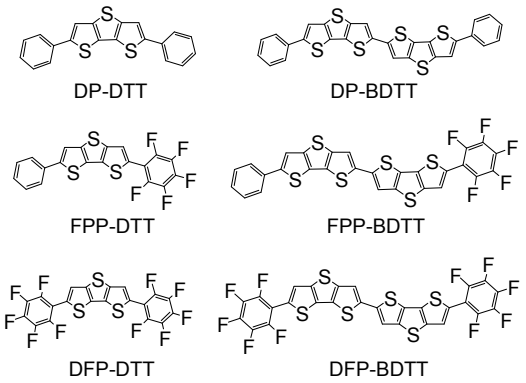

Figure 1. Chemical structures of the compounds investigated in this study

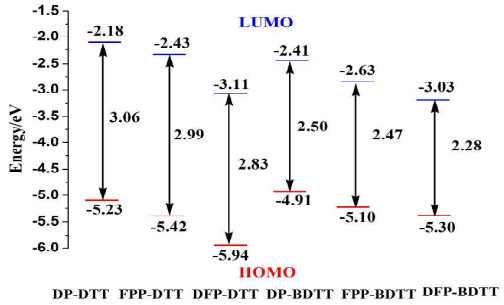

Figure 2. The HOMO and LUMO energies for the **DTT** and **BDTT** derivatives

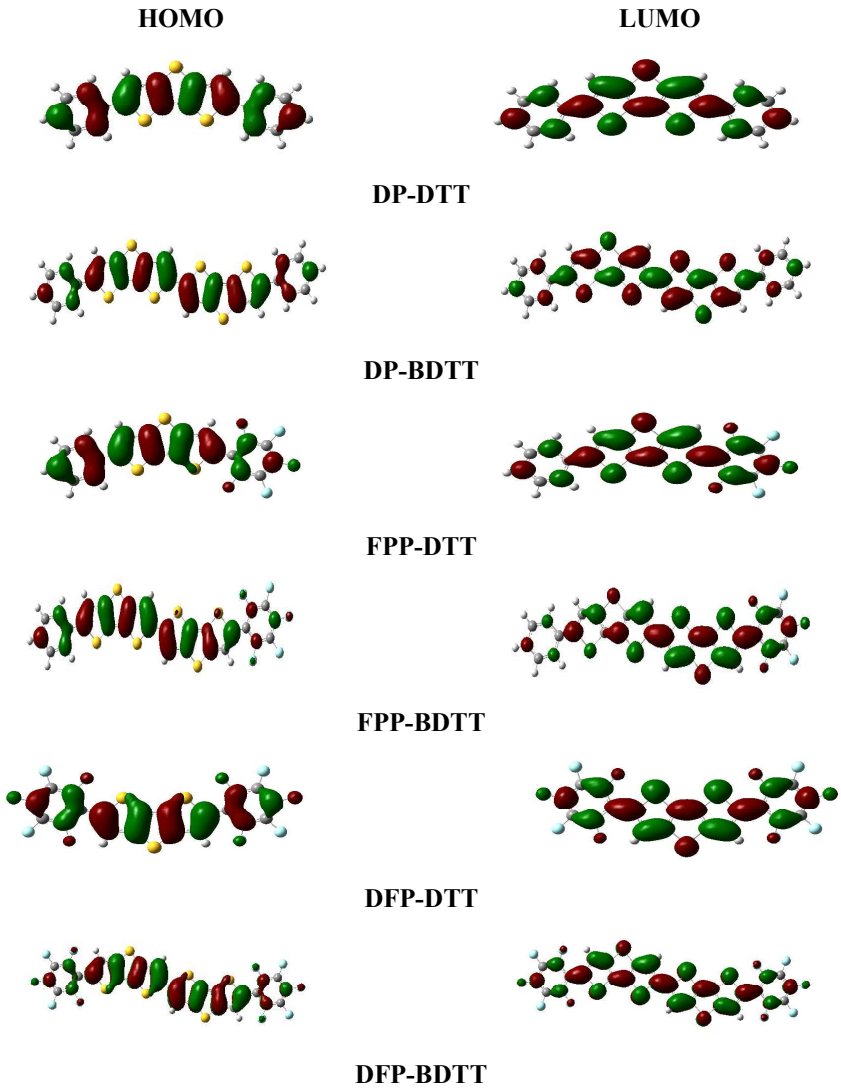

Figure 3. Distribution of HOMOs and LUMOs of the **DTT** and **BDTT** derivatives at the B3LYP/6-311G(d,p) level

Figure 4. The natural bond orbital charge population analyses of **DP-DTT** and **DFP-DTT**

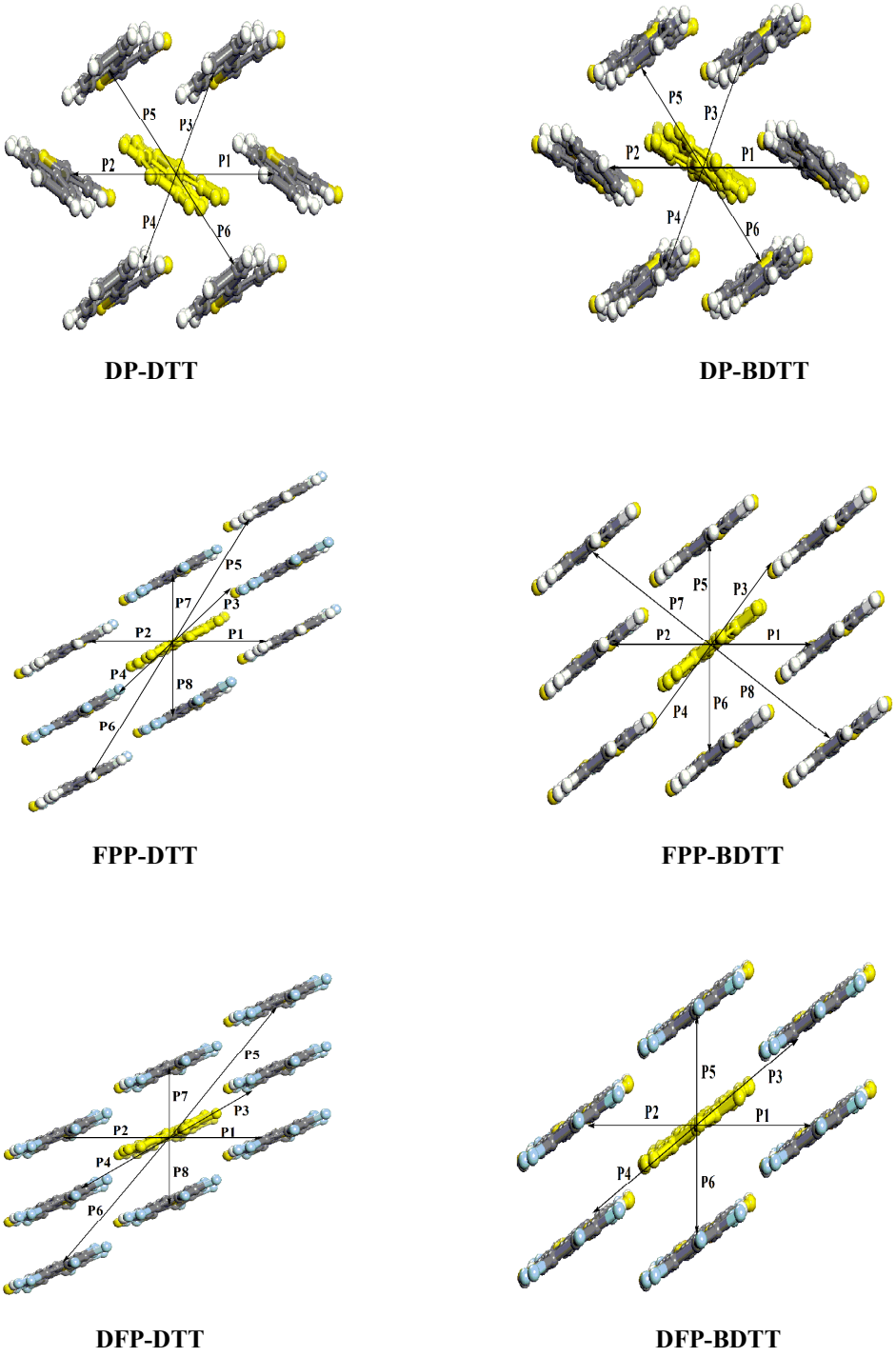

Figure 5. Main carrier hopping pathways selected based on the crystal structures for **DTT** and **BDTT** derivatives

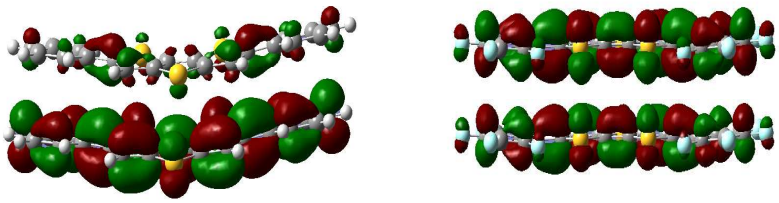

P5 P7

V_e=21.40 V_e=66.71

Figure 6. Orbital interaction of the dimer with the maximum transfer integrals (in meV) for the **DP-DTT**(left) and **DFP-DTT** (right).

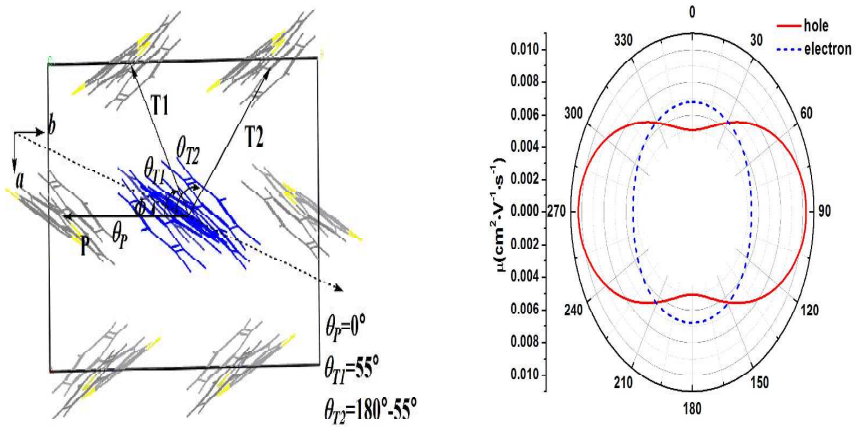

(a) (b)

Figure 7. (a) Illustration of projecting different hopping pathways to a transistor channel in *a*-*b* plane of **DP-DTT** crystal; $\boldsymbol{\theta_P}$, $\boldsymbol{\theta_{T1}}$ and $\boldsymbol{\theta_{T2}}$ are the angles of P, T1 and T2 dimers relative to the reference crystallographic axis *b*. Φ is the angle along a transistor channel relative to the reference crystallographic axis *b*. (b) the simulated hole and electron anisotropic mobilities in the *a*-*b* plane of **DP-DTT**.

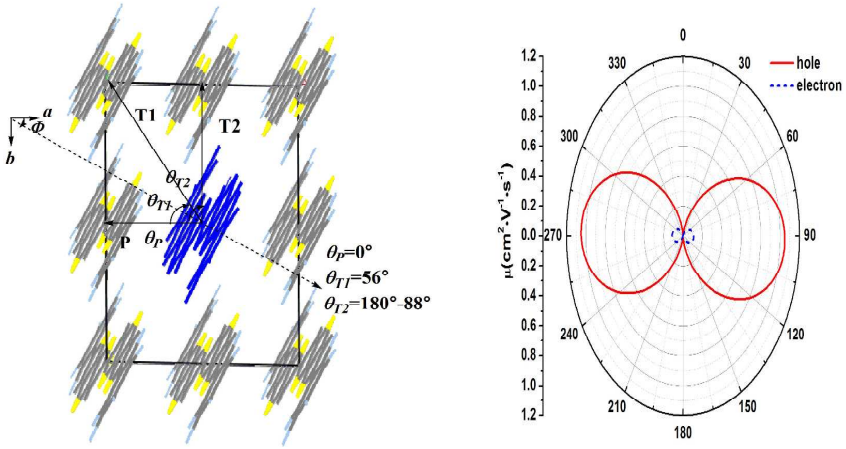

(a) (b)

Figure 8. (a) Illustration of projecting different hopping pathways to a transistor channel in *a*-*b* plane of **DFP-BDTT** crystal; θ_P, θ_{T1} and θ_{T2} are the angles of P, T1 and T2 dimers relative to the reference crystallographic axis *a*. Φ is the angle along a transistor channel relative to the reference crystallographic axis *a*. (b) the simulated hole and electron anisotropic mobilities in the *a*-*b* plane of **DFP-BDTT**.